Supplementary Data Files and Figures

Data S1. Excel spreadsheet summary data set for SILAC/TMT protein biogenesis study of Hela Cas9 parental and HeLa Cas9 SR KO cells. An Excel spreadsheet is provided listing the protein FDR confidence, Uniprot protein accession number, Uniprot protein entry name, % coverage, # of unique peptides, GO biological process, GO cellular component, GO molecular function, gene symbol, chromosomal location, KEGG pathway, reactome pathway, calculated SILAC abundance in heavy and light label, abundance ratio variability [%] (SILAC). For TMT quantitation of protein abundance, TMT light and TMT heavy datasets are provided and in addition to the information noted above, include protein abundance values for each TMT tag in each subcellular fraction: cytosol (C), peripheral membrane (P), and integral membrane (M) fractions of HeLa parental controls and SR-deficient cells. Related to **Fig. 4**.

Data S2. Excel spreadsheet summary mRNA subcellular localization and expression data set Hela Cas9 parental and HeLa Cas9 SR KO cells. An Excel spreadsheet is provided listing gene ID, species, and biological triplicate mean TPM value listings for the series: HeLa Cas9 *SRB*/siRNA SRA, HeLa Cas9 *SRB*/scramble siRNA, HeLa Cas9 *SRB* untransfected, HeLa Cas9 WT/*SRA* siRNA, HeLa Cas9 WT untransfected, HeLa Cas9 *SRB*/siRNA SRA. Each genotype conditions comprises three biological triplicate analyses as follows: HeLa Cas9 *SRB*/siRNA SRA, cytosol compartment; HeLa Cas9 *SRB*/ siRNA SRA, ER compartment, HeLa Cas9 *SRB*/siRNA SRA, total cellular RNA; HeLa Cas9 *SRB*/scramble siRNA cytosol compartment; HeLa Cas9 *SRB*/scramble siRNA, ER compartment; HeLa Cas9 *SRB*/ scramble siRNA, total RNA; HeLa Cas9 *SRB* untransfected cytosol compartment; HeLa Cas9 *SRB*/untransfected ER compartment; HeLa Cas9 SRB untransfected, total; HeLa Cas9 WT/*SRA* siRNA cytosol compartment, HeLa Cas9 WT/*SRA* siRNA ER compartment; HeLa Cas9 WT/*SRA* siRNA, Total; HeLa Cas9 WT/scramble siRNA cytosol compartment; HeLa Cas9 WT/scramble siRNA ER compartment; HeLa Cas9 WT/scramble siRNA, Total; HeLa Cas9 WT untransfected cytosol compartment; HeLa Cas9 WT/untransfected ER compartment; HeLa Cas9 WT/untransfected, Total.

Data S3. Excel spreadsheet summary data set for 4SU-seq pulse-chase studies of mRNA export and subcellular localization. An Excel spreadsheet is provided listing gene ID and spike-in normalized TPM values for biological duplicate (A, B) of 4SU-tagged mRNAs isolated at the 15', 30', 45', and 60' time points for the cytosol (Cyto) and endoplasmic reticulum (ER) subcellular fractions. For the translation inhibitor studies (single time point)(Inhibitor), an Excel spreadsheet is provided listing gene ID and 4SU-mRNA TPM counts in the cytosol and ER fractions at 45 min.

Data S4.
Excel spreadsheet summarizing up- and down-regulated genes at FC $\geq$2 in primary cell genotype conditions examined in the study.

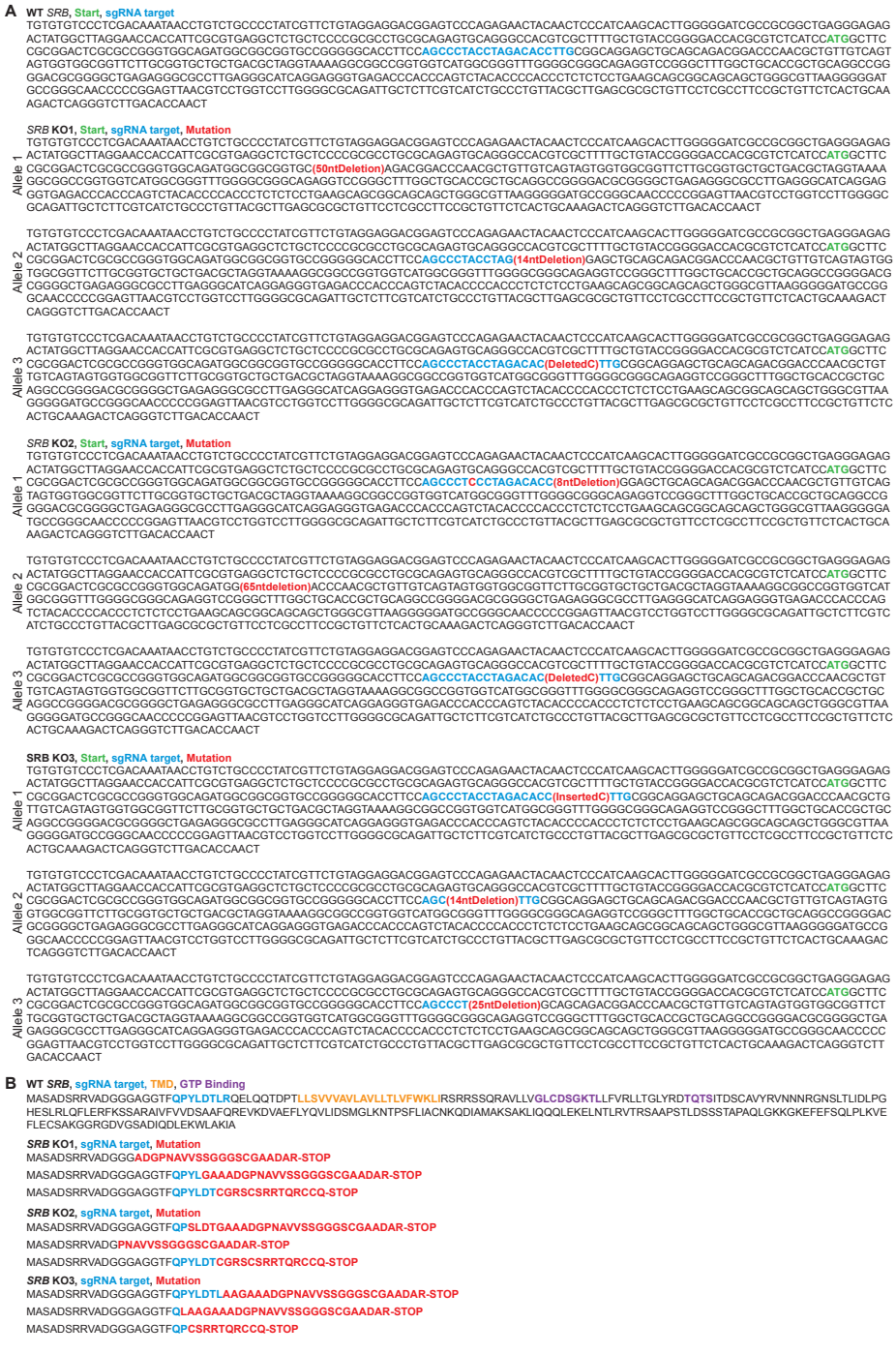

Figure S1. Genomic sequencing of CRISPR-edited *SRB* and predicted amino acid sequence of mutated gene. A) As described in Methods, genomic *SRB* PCR products were sequenced following Zero Blunt® TOPO® cloning (Thermo-Fisher) at frequencies sufficient to identify mutations in all alleles. **B)** predicted translation products for CRISPR-edited *SRB* alleles. The mutant sequences are depicted, ending at the STOP codon.

Exon #	Position on Gene	Length (nt)	Coding (AA)
1	21793-21980	188	Met1-Val52
2	22587-22681	95	Val52-Arg83
3	23724-23801	78	Leu84-Arg109
4	27905-27177	83	Gly110-Arg137
5	31568-31704	137	Arg137-Asp183
6	32856-32910	55	Asp183-Leu201
7	35531-37470	1940	Leu201-Ala271

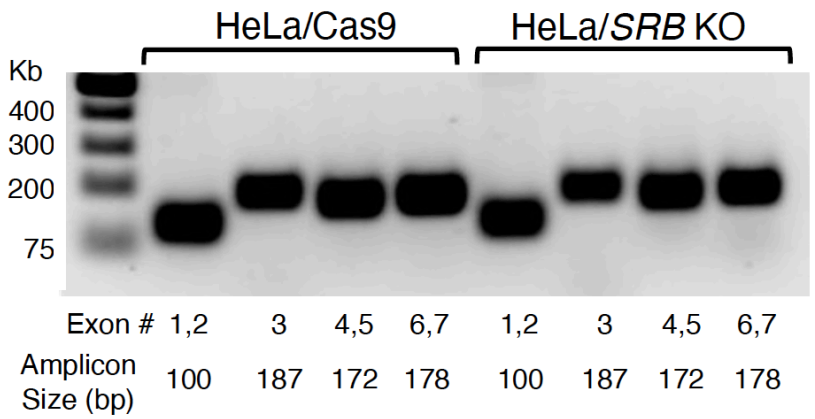

Figure S2. Screen for splice variants in CRISPR-edited *SRB* transcripts. Total RNA was isolated from HeLa Cas9 parental and HeLa *SRB* KO #2 cells and screened for intron retention/exon skipping by PCR analysis. Genomic exon positions, length (nt), and coding sequences are provided. A digital image of the PCR analysis is depicted, with the target exon and predicted amplicon size indicated. Intron spanning amplicons are indicated by the two-exon notation.

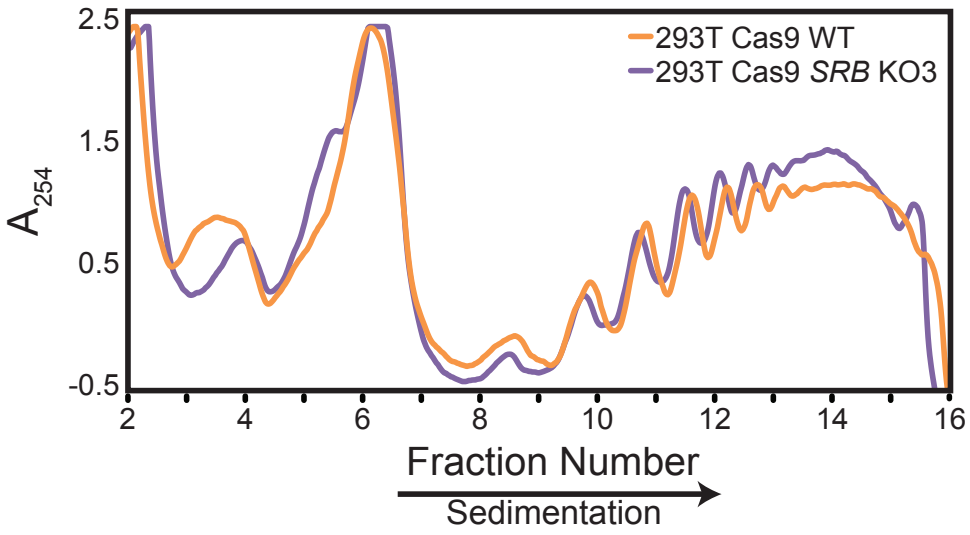

Figure S3. Polysome profile of 293T-*SRB* KO cells. Polysomes from 293T *SRB* KO cells were analyzed as described in Methods. A digital trace of the A_{254} nm absorbance profile of the parental 293T Cas9 and 293 *SRB* KO3 cells is depicted.

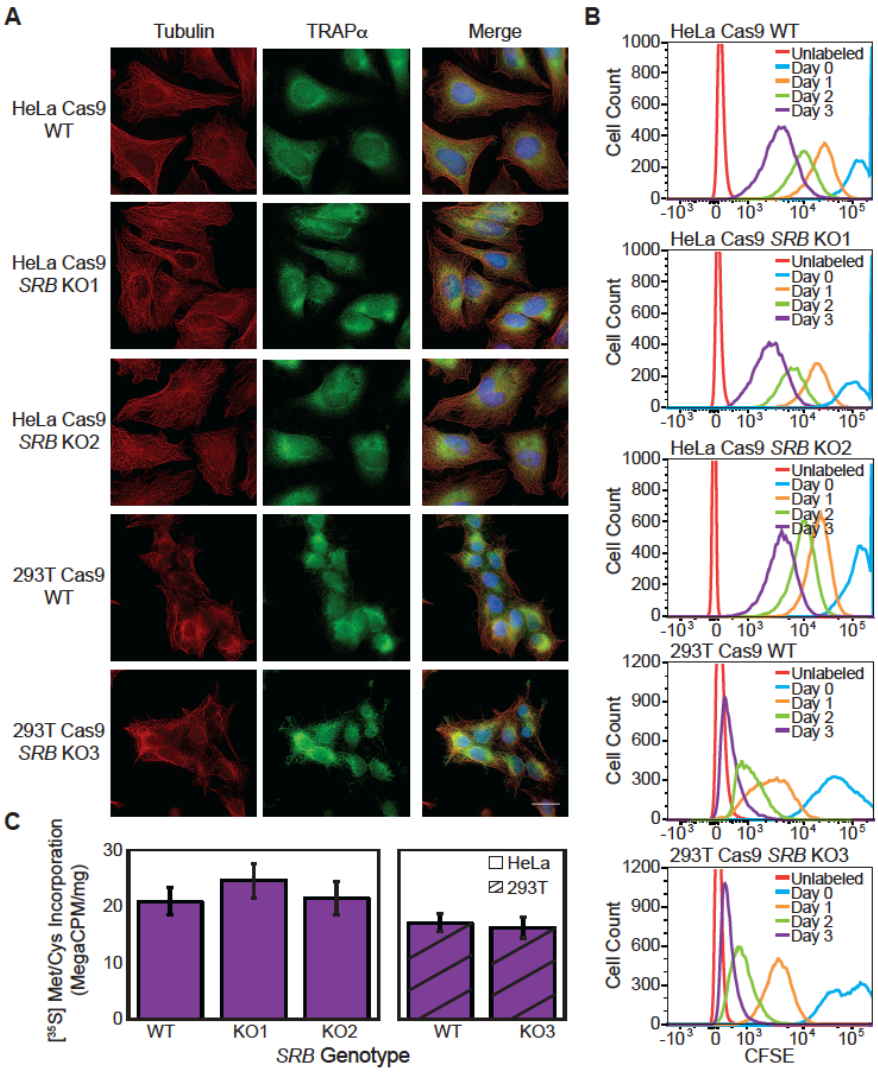

Figure S4. Cell morphology, doubling time, and protein synthesis rates for clonal HeLa *SRB* KO and 293T *SRB* KO cell lines. A) Cell structure and morphology were examined by immunofluorescence staining for the microtubule network (tubulin) and ER (TRAPα). **B)** Cell proliferation was assessed flow cytometry using the CFSE doubling/dilution method as per manufacturer's recommendation. Data was visualized using FlowJo software (BD Biosciences). **C)** Protein synthesis rates were determined by [^{35}S] methionine/cysteine incorporation, where cell monolayers were labeled with [^{35}S] methionine/cysteine, rinsed in cycloheximide-supplemented PBS, detergent lysed, proteins collected by TCA precipitation, acetone washed, resuspended in SDS sample buffer and radioactivity determined by liquid scintillation counting. Protein concentrations were determined by BCA assay. Data are reported as counts per minute (cpm) per milligram (mg) of protein for experimental samples minus average cpm/mg of cycloheximide controls.

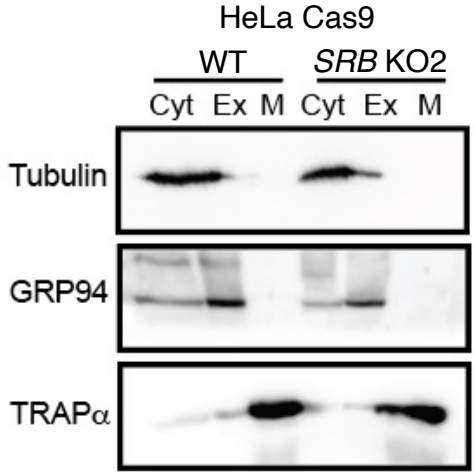

Figure S5. Marker protein distribution analysis of cell fractionation efficacy. Equivalent volumes of the cytosol, peripheral membrane protein, and integral membrane protein fractions were TCA-precipitated, separated by SDS-PAGE, and the distribution of a cytosolic protein (GAPDH), membrane protein (TRAPα), and ER luminal protein (GRP94) determined by immunoblot. C = cytosol; Ex = urea/carbonate extractable fraction, and M = membrane proteins fraction.

A

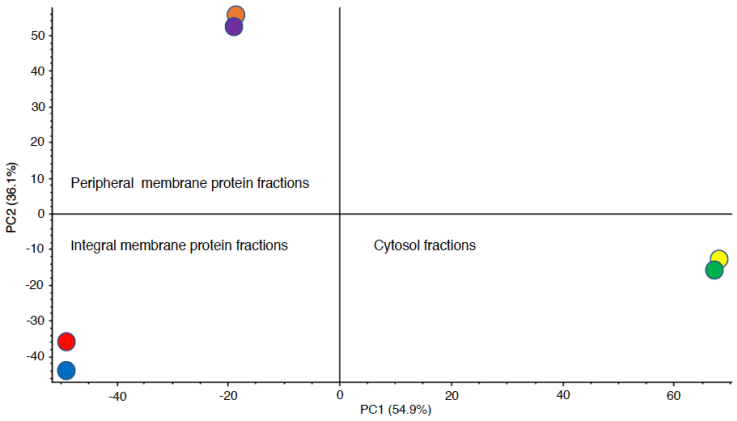

B

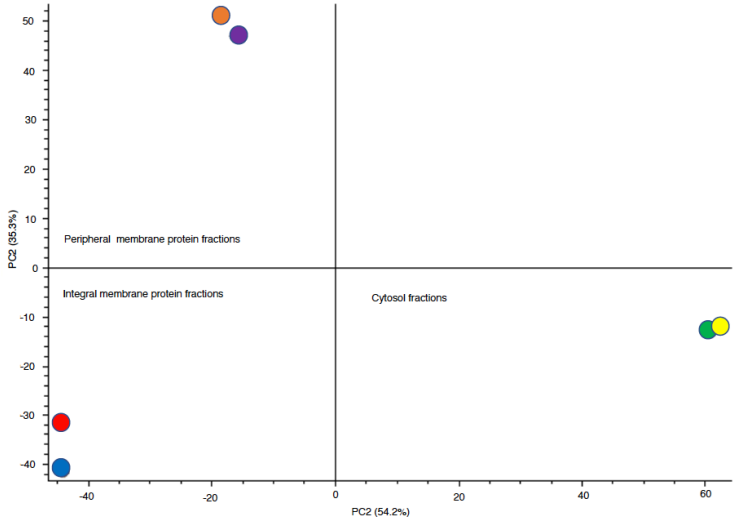

Figure S6. Principal component analysis of protein compositions of subcellular fractions. To determine the reproducibility of the protein fractionation methods used for examining protein biogenesis in HeLa Cas9 and HeLa SR KO cells, a principal component analysis of the proteomics data set was performed, comparing the protein compositions of the membrane, peripheral membrane, and cytosolic protein fractions. **A)** Light SILAC-labeled; **B)** Heavy SILAC-labeled. For both PCA plots, membrane fraction (blue, red), lower left quadrant, peripheral protein fraction (purple, orange), upper left quadrant, and cytosolic fraction (green, yellow), lower right quadrant.

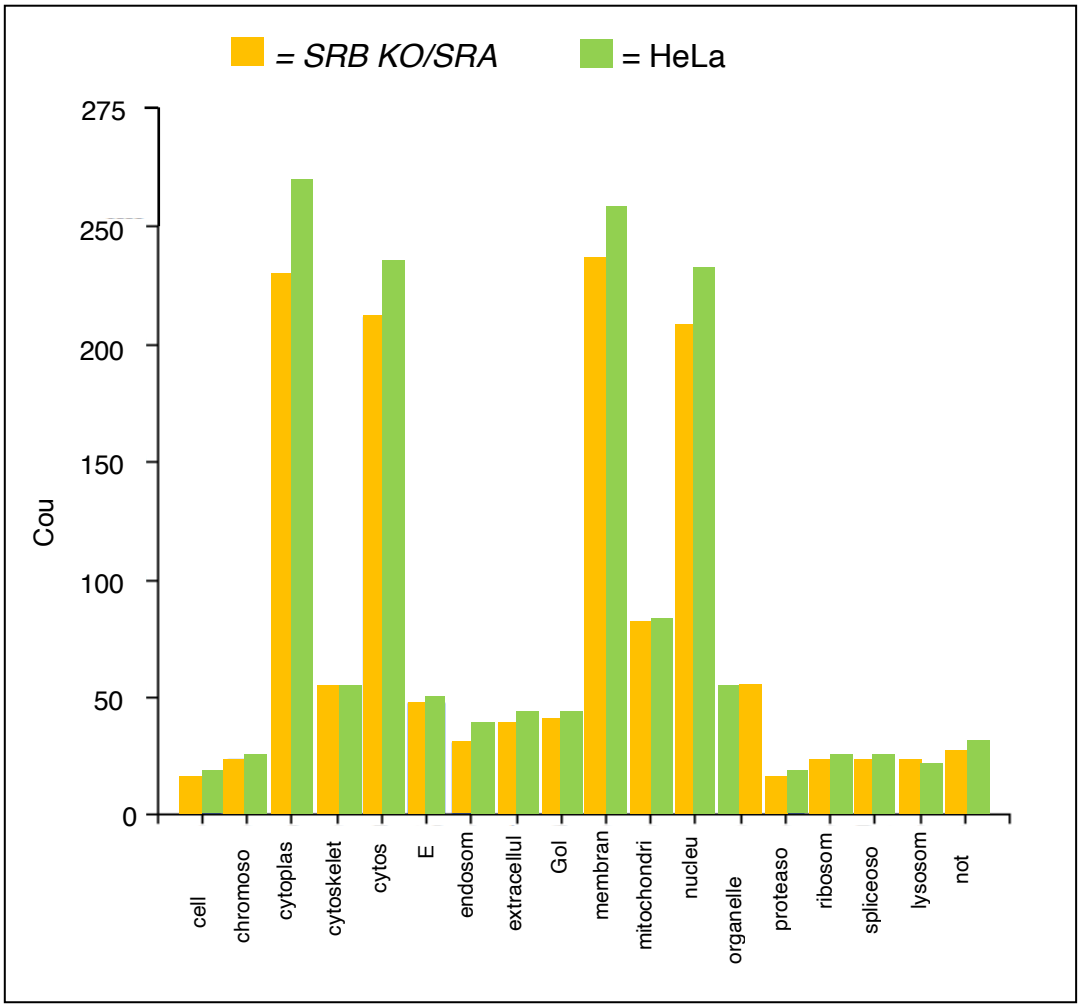

Figure S7. Comparison of protein compositions of HeLa Cas9 and HeLa SR KO cells by subcellular distribution. GO cellular component protein assignments were used to display the overall protein compositions of the parental HeLa Cas9 and HeLa SR KO cells. Data derived from **Supplementary Data S1**, which includes protein abundance values for each TMT tag in each subcellular fraction: cytosol, peripheral membrane, and integral membrane fractions of HeLa parental controls and SR-deficient cells and GO cellular component assignments

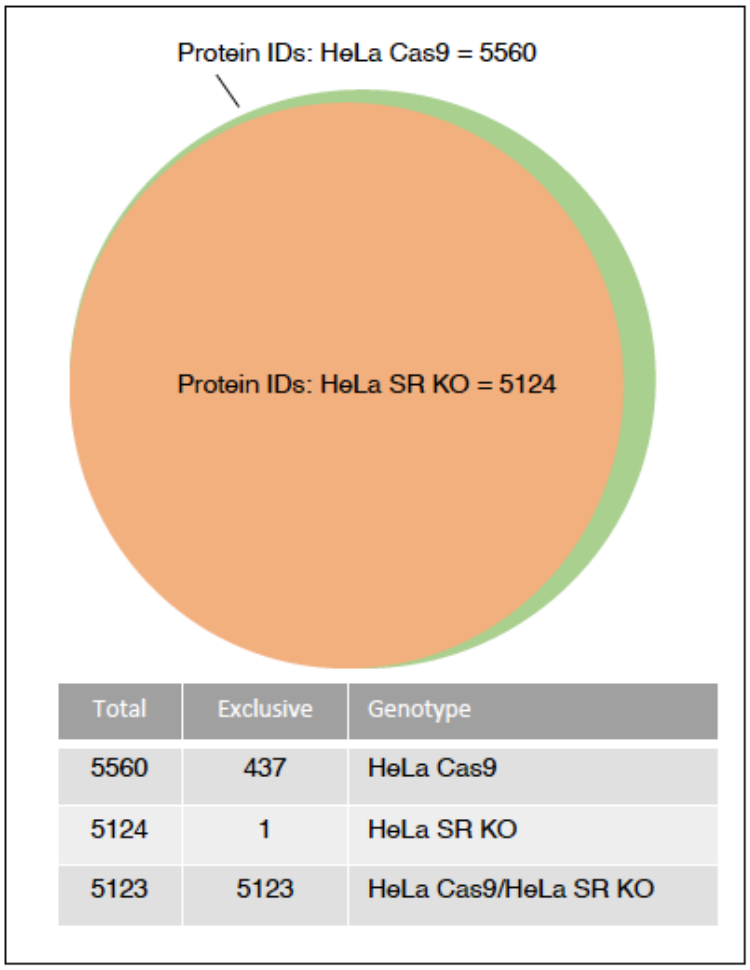

Total	Exclusive	Genotype
5560	437	HeLa Cas9
5124	1	HeLa SR KO
5123	5123	HeLa Cas9/HeLa SR KO

Figure S8. Summary proteomic identification statistics for HeLa Cas9 and HeLa SR KO cells. A Venn diagram is provided depicting the total number of proteins identified in the HeLa Cas9 and HeLa SR KO cells, including total number of proteins identified as well as shared and exclusive proteins identified.

A

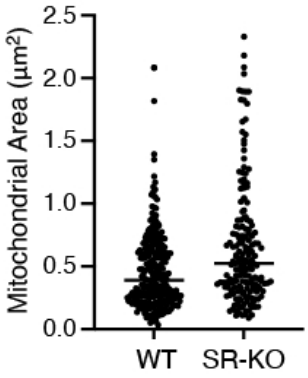

B

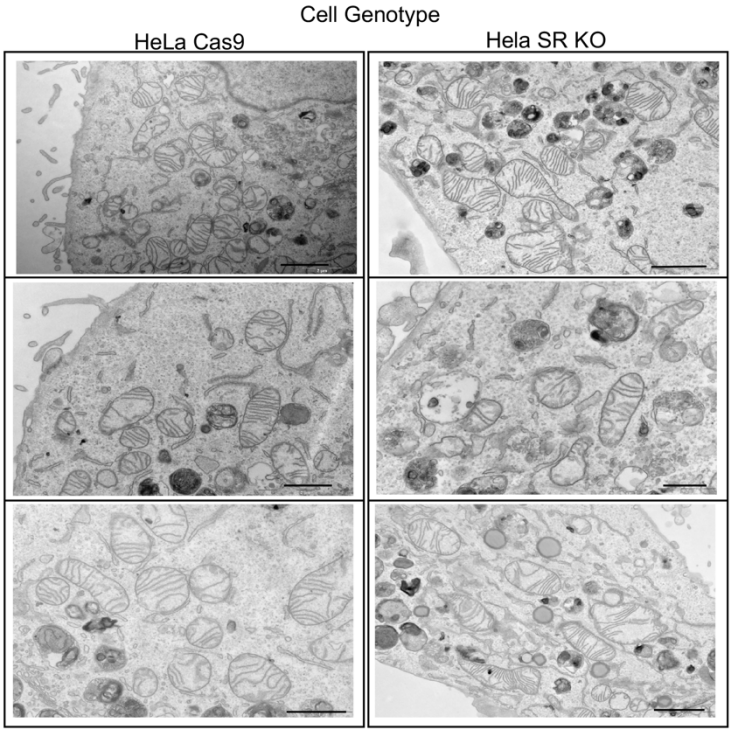

Figure S9. Analysis of mitochondrial surface area and morphology in control and SR KO cells. HeLa Cas9 parental cells and HeLa Cas9 *SRB* KO cells were cultured, transfected with *SRA*-targeting siRNA or a non-targeting siRNA and at 96 hr post-transfection fixed with glutaraldehyde/sodium cacodylate buffer. Samples were processed for transmission electron microscopy and electron micrographs obtained on a FEI Tencai BioTwin TEM. Micrographs were blinded and mitochondrial surface areas determined using Image J, by the method of Lam et al. (Lam et al. 2021). 120-150 individual mitochondria were quantified for each condition. **A)** individual and mean mitochondrial surface area values for HeLa Cas9 and HeLa Cas9 *SRB* KO cells. Plots were generated and statistical analysis performed using Prism-GraphPad software. **B)** Digital images of representative thin section micrographs of HeLa Cas9 and HeLa Cas9 *SRB* KO cells, illustrating mitochondrial dimensions and morphologies. Scale bar = 2 μm.

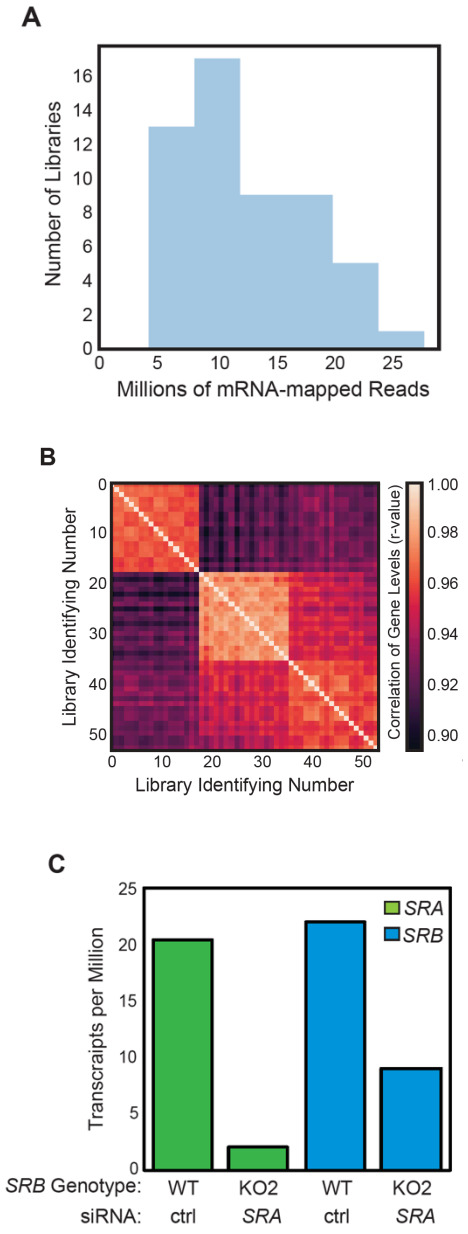

Figure S10. RNAseq library metrics for RNAseq analysis of HeLa Cas9, HeLa Cas9 + non-targeting siRNA, HeLa Cas 9 + *SRA*-targeting siRNA, HeLa *SRB* KO, HeLa *SRB* KO + non-targeting siRNA, and HeLa *SRB* KO + *SRA*-targeting siRNA. Biological triplicate RNAseq analyses of each cell genotype and experimental condition were performed. **A)** histogram of mapped read depth distribution of RNAseq library suite. **B)** Paired correlation plot depicting gene level correlation metrics between library pairs. **C)** *SRA* and *SRB* mRNA abundance in the parental HeLa Cas9 and HeLa Cas9 *SRB* KO cells +/- transfection with *SRA*-targeting siRNA.

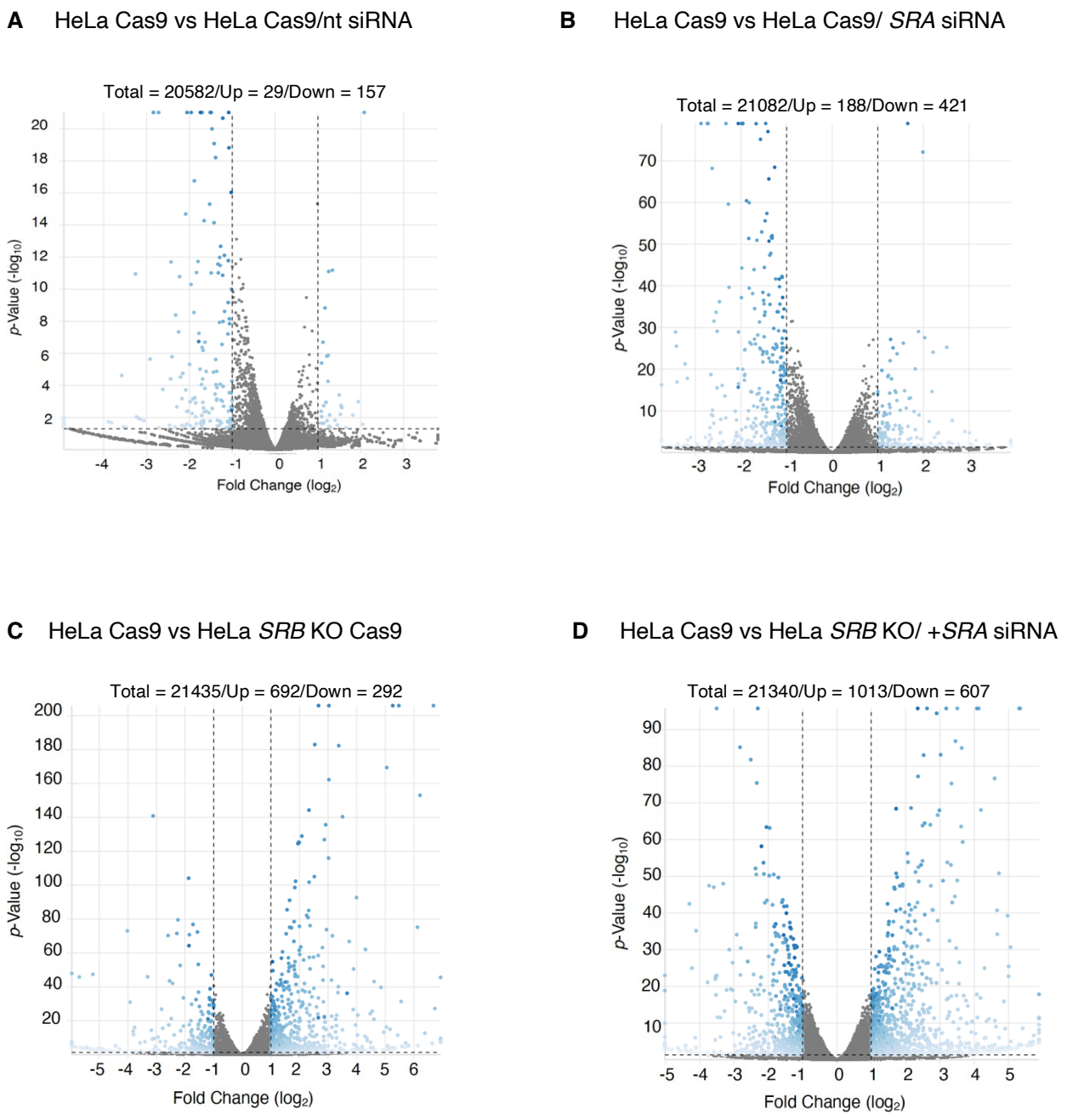

Figure S11. Differential gene expression analysis of transcriptomic response to loss of SR expression. RNAseq datasets were analyzed for differential gene expression in response to transfection with non-targeting siRNA, transfection with *SRA*-targeting siRNA, and combined *SRB* KO/*SRA* KD. Depicted are volcano plots with number of identified genes and up- and down-regulated gene numbers, determined at a fold-change cutoff value of 2 (log_2=1). Differential gene expression analysis performed with DESeq2. **A**) HeLa Cas9 vs HeLa Cas9/nt siRNA, **B)** HeLa Cas9 vs HeLa Cas9/ *SRA* siRNA, **C)** HeLa Cas9 vs HeLa *SRB* KO Cas9, **D)** HeLa Cas9 vs HeLa *SRB* KO/ +*SRA* siRNA.

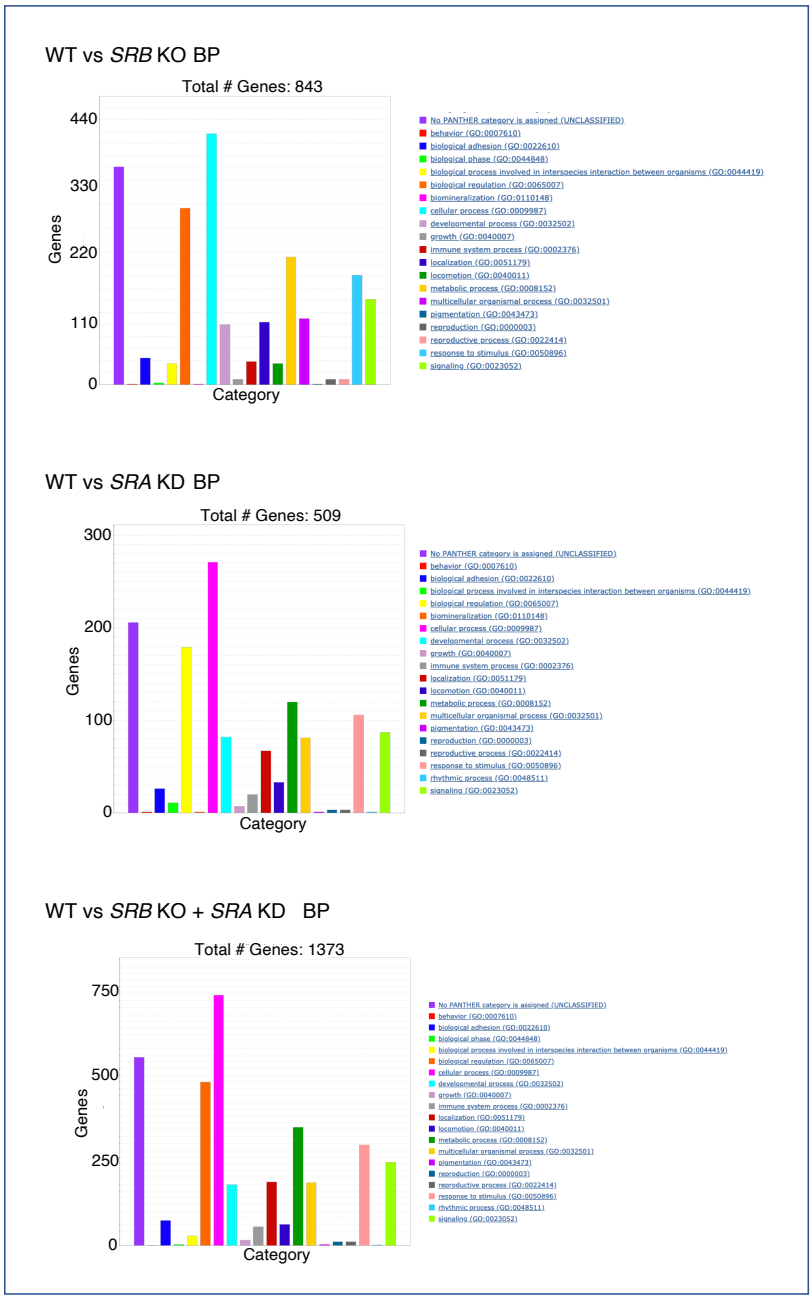

Figure S12. Panther GO analysis of differential gene expression patterns between parental and gene-edited HeLa cells. Depicted are Panther GO output enrichments for Biological Process gene subontologies, comparing parental HeLa Cas9 with HeLa Cas 9 + *SRA*-targeting siRNA, HeLa *SRB* KO, and HeLa *SRB* KO + *SRA*-targeting siRNA.

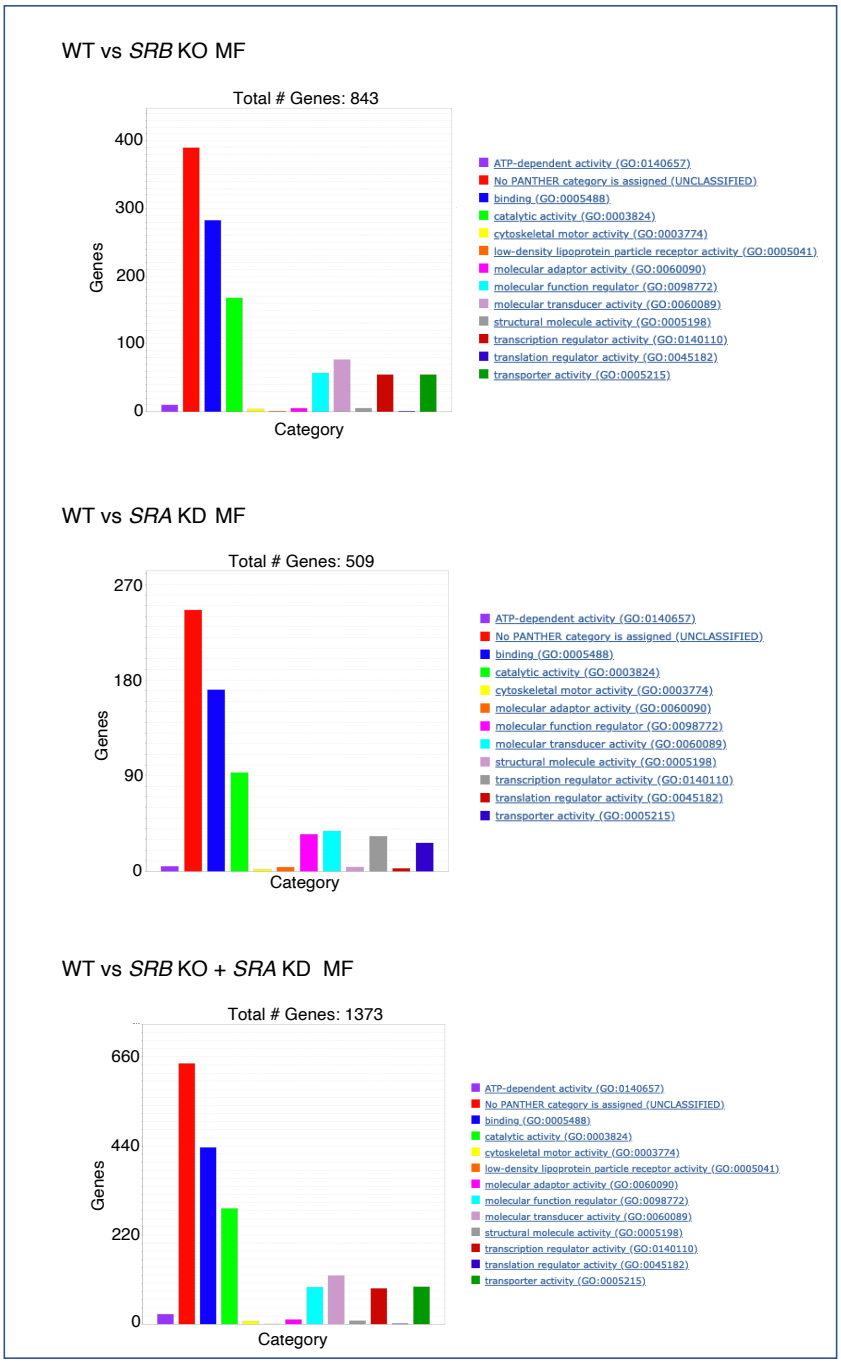

Figure S13. Panther GO analysis of differential gene expression patterns between parental and gene-edited HeLa cells. Depicted are Panther GO output enrichments for Molecular Function gene subontologies, comparing parental HeLa Cas9 with HeLa Cas 9 + *SRA*-targeting siRNA, HeLa *SRB* KO, and HeLa *SRB* KO + *SRA*-targeting siRNA.

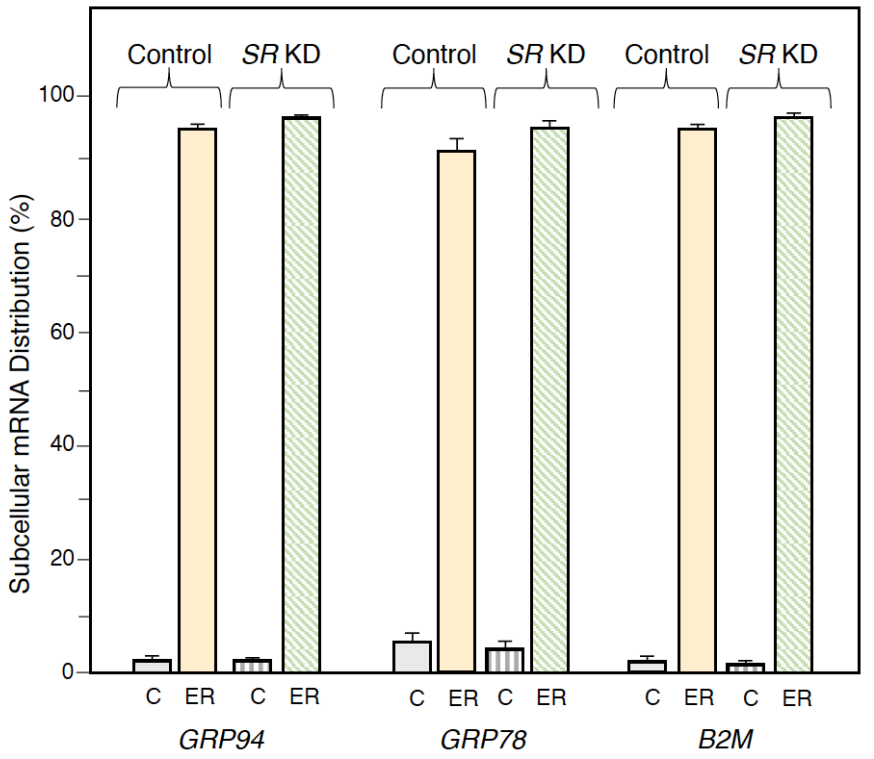

Figure S14. Signal sequence-encoding mRNAs are efficiently localized to the endoplasmic reticulum in siRNA *SRA*/*SRB* knockdown HeLa cells. HeLa Cas9 cells were transfected with either a non-targeting siRNA or pooled *SRA*/*SRB* siRNAs and at 96 hr post siRNA transfection separated into cytosol and ER (membrane) fractions by sequential detergent extraction. Total RNA was isolated from the subcellular fractions and the relative fractional abundance of the signal sequence-encoding mRNAs *GRP94*, *GRP78*, and *B2M* in the cytosol (C) and membrane (ER) fractions were determined by RT-qPCR, using cell equivalent volumes of the total RNA fractions for reverse transcription. Control experiments with non-targeting siRNA transfection were indistinguishable from non-transfected cells. Experiments were conducted in biological triplicate with technical duplicates performed for each analysis. Values represent mean +/- S.D. *SRA* and *SRB* siRNA mRNA knockdown efficiencies were determined by RT-qPCR; knockdown efficiencies were 71 $\pm$ 3% for *SRA* and 75 $\pm$ 0.4 % for *SRB*.

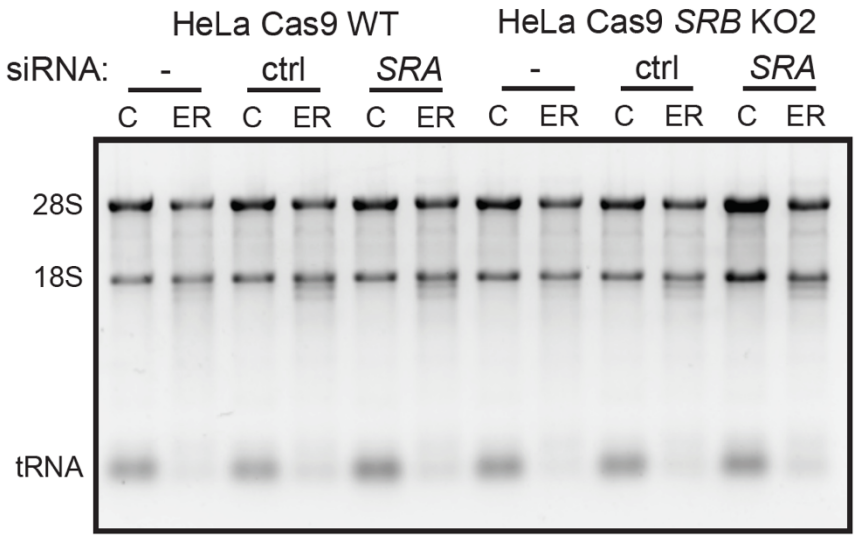

Figure S15. Steady-state subcellular ribosome distributions in HeLa Cas9 and HeLa SR KO cells. HeLa Cas9 and HeLa SR KO cultures (96 hr post siRNA transfection) were separated into cytosol and ER (membrane) fractions by sequential detergent extraction and ribosome fractions isolated by ultracentrifugation. Total RNA was isolated from ribosome pellets and equivalent fractional sample volumes analyzed for 18S and 28S ribosomal RNA and tRNA subcellular distributions by denaturing agarose gel electrophoresis.

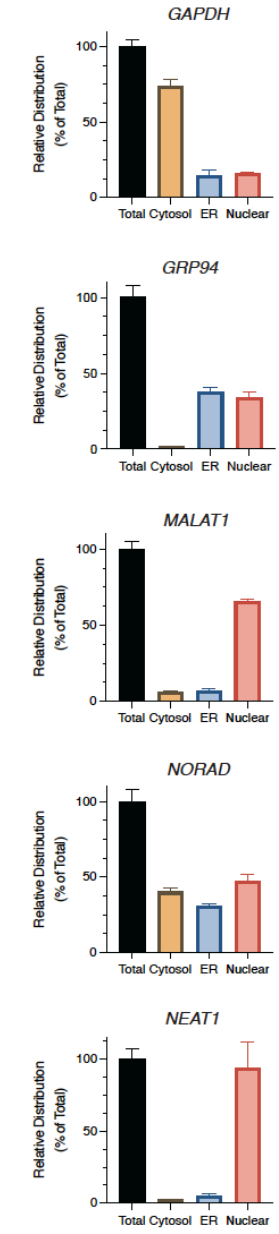

Figure S16. Validation of three compartment subcellular fractionation protocol. To assess the selectivity of the three-compartment subcellular fractionation protocol, lncRNA distributions were determined by qRT-PCR, examining the fractional distributions of a cytosolic compartment enriched mRNA (*GAPDH)*, ER-enriched mRNA (*GRP94)*, the lncRNAs *MALAT1*, *NEAT1* as representative nucleus-localized lncRNAs, and *NORAD*, a shuttling lncRNA. The cytosol, ER (membrane), and nuclear fractions of HeLa *SRB* KO cells. Cell cultures were fractionated by sequential detergent extraction and total RNA isolated by Trizol extraction. Biological triplicate cell fractionations were performed, and qPCR values normalized to total (sum of all fractions).

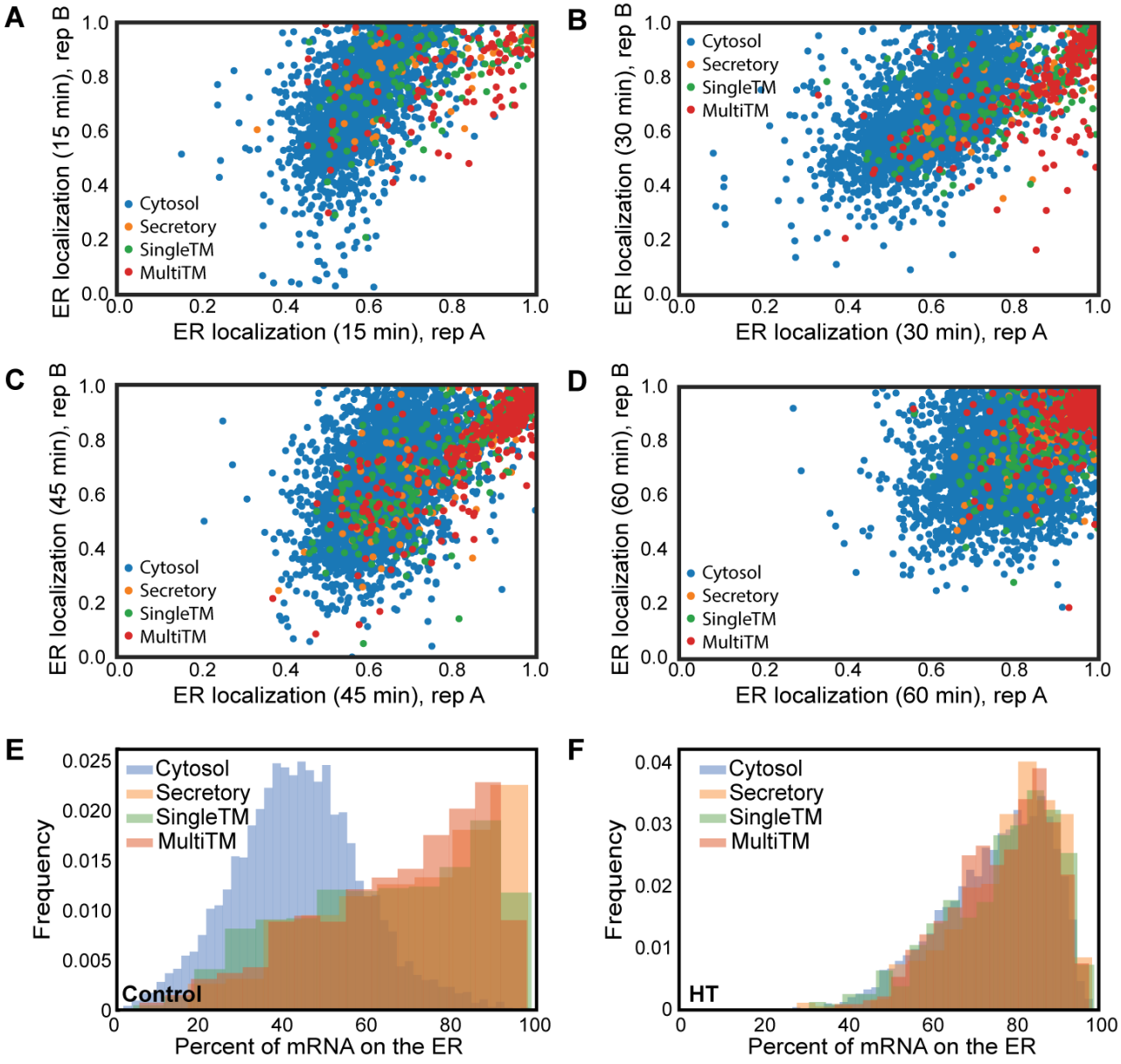

Figure S17. Composite 4SU-seq analysis of 4SU-mRNA export time course and subcellular distribution in control and translation initiation-inhibited HeLa Cas SR KO cells. A-D) Panels depict gene 4SU-mRNA subcellular distributions at 15', 30', 45', and 60' time points comparing two independent biological replicates. **E,F)** Depicted are the subcellular mRNA distributions expressed as fractional enrichment on the ER, in control (**E**) and translation initiation inhibitor (harringtonine)-treated (**F**) HeLa SR KO cells.